Chemical Engineering Research and Design xxx (xxxx) xxx–xxx

Available online at www.sciencedirect.com

Chemical Engineering Research and Design

journal homepage: www.elsevier.com/locate/cherd

A new approach to analyze the equilibrium and transient behaviors of particulate systems and the subsequent application to multiphase fluid systems

Moein Assar, Brian Arthur Grimes *

Ugelstad Laboratory, Department of Chemical Engineering, Norwegian University of Science and Technology (NTNU), N-7491 Trondheim, Norway

ARTICLE INFO

Article history:
Received 9 June 2022
Received in revised form 25 October 2022
Accepted 26 October 2022
Available online xxxx

Keywords:
Population balance equation
Multiphase fluid
Particulate system
Orthogonal Collocation
Approximation technique

ABSTRACT

Fast and robust computation for population balance models is a crucial requirement for simulating particulate systems. Despite all the recent advances in developing relevant computational algorithms, either efficiency or robustness can only be achieved at the expense of the other. However, optimal compromise is possible by having prior estimates of the system's internal length and time scales. Thus, an approximation technique is introduced in this study to extract equilibrium and transient behaviors for a particulate system considering coalescence and breakage phenomena. The approximation method is developed by simplifying assumptions on the available analytical solution for a spatially homogeneous population balance equation with simple kernels. The derived equilibrium and transient equations suggest that the system is governed by a dimensionless group that can describe the equilibrium distribution of the system as well as the rate and the direction that the system is likely to evolve. The method is applied to two different sets of complex breakage and coalescence kernels used for liquid-liquid dispersed systems. The approximated time and length scales were validated with numerical results; thus, the approximation can be used to generate targeted element-based orthogonal collocation grids for fast and robust computation of transient and steady-state particulate systems. This approach can significantly decrease the computation time, typically by 40–70 % for steady-state conditions.

1. Introduction

Population balance modeling has been widely used throughout past decades as the main backbone to describe particulate systems via evolution of the particle size distribution as well as functions of system operating conditions and physicochemical properties (Ramkrishna, 2000). Such models are used frequently in different areas such as crystallization, microbial cell growth, granulation, polymerization, and multiphase fluid systems to support process design, optimization, and control (Falola et al., 2013; Qamar, 2014). Notably, the population balance equation (PBE) is the primary tool to simulate separation and transport processes involving multiphase fluids by applying fundamental knowledge regarding coalescence and breakage phenomena. Such simulations aim to predict the evolution of droplet size distribution (DSD) formed by breakage and coalescence phenomena that might significantly impact equipment performance.

* Corresponding author.
E-mail address: brian.a.grimes@ntnu.no (B.A. Grimes).

https://doi.org/10.1016/j.cherd.2022.10.044

Nomenclature

c	Constant coalescence rate in analytical solution (m^3s^{-1}).
c_{est}	Estimated constant coalescence rate (m^3s^{-1}).
C_1, C_2	Tuning parameters used in approximation of transient time.
$f_{n,r}$	Radius-based number density function (m^{-4}).
$f_{n,v}$	Volume-based number density function (m^{-6}).
$f_{v,r}$	Radius-based volume density function (m^{-1}).
$\hat{f}_{v,r}$	Dimensionless radius-based volume density function ($f_v r_m$).
g	Breakage frequency (s^{-1}).
k	Coalescence rate (m^3s^{-1}).
k_{c1}, k_{c2}	Tuning parameters used in coalescence model.
k_{b1}, k_{b2}	Tuning parameters used in breakage model.
k_1	Time-dependent coefficients used in the analytical solution (m^{-6}).
k_2	Time-dependent coefficients used in the analytical solution (m^{-3}).
$\hat{k}_1$, $\hat{k}_2$	Dimensionless time-dependent coefficients used in the analytical solution.
m_0	0th order moment equal to number of droplets per unit volume (m^{-3}).
m_3	3rd order moment.
M	Dimensionless group number.
N	Number of droplets per unit volume (m^{-3}).
$\hat{n}$	Dimensionless time-dependent coefficient used in the analytical solution.
r	Droplet radius (m).
$\hat{r}$	Dimensionless droplet radius (r/r_m).
r_m	Upper bound of droplet radius internal domain (m).
s	Parameter used in breakage frequency kernel ($m^{-3}s^{-1}$).
s_{est}	Estimated parameter used in breakage frequency kernel ($m^{-3}s^{-1}$).
t	Time (s).
$\hat{t}$	Dimensionless time (t/t_c).
t_c	Characteristic time (s).
v	Droplet volume (m^3).
v_m	Upper bound of droplet volume internal domain (m^3).
β_r	Radius-based daughter distribution (m^{-1}).
β_v	For volume-based daughter distribution (m^{-3}).
Γ	Gamma function.
Γ^{-1}	Inverse gamma function.
δ	Dirac delta function.
μ_r	Average droplet radius (m).
$\hat{\mu}_r$	Dimensionless average droplet radius.
σ_r	Droplet radius standard deviation (m).
$\hat{\sigma}_r$	Dimensionless droplet radius standard deviation.
ϕ	Volume fraction.
ε	Turbulent energy dissipation rate (m^2s^{-3}).
τ	Dispersed phase surface tension (Nm^{-1}).
ρ_c	Continuous phase density (kgm^{-3}).
ρ_d	Dispersed phase density (kgm^{-3}).
ψ_E	Collision efficiency used in coalescence rate model.
ω	Coalescence efficiency used in coalescence rate model (m^3s^{-1}).

One powerful class of methods for solving PBE is the weighted residue methods (MWR). They have the so-called infinite order of accuracy comparing to other methods such as class methods, finite volume method, and finite element method (FEM) (Mantzaris et al., 2001a), as well as better convergence behavior (Solsvik and Jakobsen, 2012). These properties can increase the computational efficiency as normally coarser grids can adequately provide the same accuracy compared with other methods (Dorao and Jakobsen, 2006). Here, the dependent variable (i.e. DSD) is approximated with a truncated series of so-called trial function over the entire computational domain subject to minimization of the product of the governing equation with the test function (Mantzaris et al., 2001a). Several spectral methods have been proposed based on the choice of trial and test functions, namely Galerkin, Tau, collocation, and least square. In collocation methods, the test function is a Dirac delta function, assuring exact satisfaction of equation at the collocation points (Mantzaris et al., 2001a). Moreover, the collocation method provides the simplest and most computationally efficient scheme with accuracy and stability similar to the Galerkin method (Mantzaris et al., 2001a; Solsvik and Jakobsen, 2013). To add more flexibility to these methods, several researchers have also used MWR in an element-based framework (Costa et al., 2018; Gelbard and Seinfeld, 1978; Mahoney and Ramkrishna, 2002; Mantzaris et al., 2001b; Nicmanis and Hounslow, 1998, 1996; Rigopoulos and Jones, 2003; Zhu et al., 2009).

The current study is part of a bigger effort in which a modular C++ model library (PBmulib) is being developed based on a population balance modeling approach for separation and transport of multiphase fluids in the form of crude oil and water emulsions. According to the level of complexity in the systems as well as the physics involved, these models are developed for 0, 1, and 2 spatial dimensions. These three modules can cover wide applications ranging from multiphase pipe flow to batch settlers/skimmers and 3-phase separators. The structure of the library facilitates a modular design and development for building more complex processes fast. Additionally, leveraging a C++ core ensures fast computation speeds on modern platforms. The library will allow the PBE models to be readily incorporated into common general-purpose or specialized simulation software environments such as MATLAB, Python, and HYSYS.

The main challenge for developing such a library is the ability to perform fast and robust computations to solve equilibrium and transient population balance models. This is compromised by the inherent numerical challenges associated with the PBE. A good description of such challenges is presented by Rigopoulos and Jones (2003); Zhu et al. (2008), which can be summarized as follows:

- Proper choice for truncation of the PBE internal domain.
- Internal consistency of the numerical schemes.
- Efficient computation of equilibrium distributions.

- Strong non-linear behavior introduced by the coalescence terms resulting in a complex convergence behavior.

Mathematically, the internal coordinate of the PBE expands to infinity. Thereby, for numerical computation, the upper bound of the internal coordinate should be truncated by a finite value. Choice of truncation point can drastically affect the accuracy of the solution as well as the stiffness of the equations. If underestimated, solution methods would fail to produce correct results. Whereas, in the case of overestimation, it would lead to poor results as wider domain ranges demand finer grids. Additionally, a stiffer system of ODEs would be expected, which consequently results in low computational efficiency. This takes place as tiny values in the tail region can attain large particle volumes, making the numerical convergence computationally costly (Nicmanis and Hounslow, 1998). Furthermore, in cases where the system of interest is in equilibrium, the equilibrium distribution is often obtained indirectly by allowing the transient system to evolve over time until it reaches equilibrium. This is usually the case when the equations are highly nonlinear and a steady-state solution cannot be obtained directly (Rigopoulos and Jones, 2003). For such problems, having a rough estimation for system transient time can be extremely valuable since many of the available numerical schemes can suffer from accumulated error and lack of internal consistency in excessive numerical time integration.

Reviewing the available literature, the solutions for this challenge can be categorized into two main approaches (Rigopoulos and Jones, 2003):

- Adopting a fixed grid technique, monitoring the solution, and changing the domain bound if required.
- Applying an adaptive or moving grid by remeshing algorithms.

The conventional fixed grid techniques require firm reliance on the user post interpretation of the results and reselection of the domain bound in case of unphysical results. Attarakih et al. (2004) developed a technique to estimate the total finite domain error. In their approach, the error is checked at each integration step; once the tolerance is violated, the calculations are stopped and restarted again with improved estimation of lower and upper bounds of the domain. However, in this method, the grid is preliminarily generated according to the initial and/or inlet distributions, and for cases with the equilibrium distribution located away from those known distributions, it requires multiple trial and error iteration to modify the grid. Such an approach can be computationally expensive.

The other alternative is to track the changes in the distribution function via a moving grid technique. Several techniques with such a strategy have been proposed by different researchers (Attarakih et al., 2002; Briesen, 2009; Duarte and Baptista, 2007; Lee et al., 2001; Sewerin and Rigopoulos, 2017). However, despite the robustness these techniques offer, the extra computational overhead can be high compared to their counterpart fixed grid techniques due to the required interpolation step involved.

From this brief overview, preliminary information about the equilibrium and transient behavior of the problem can be valuable. A preliminary estimation of the equilibrium distribution, together with the initial/inlet distribution information, can be used to make the fixed grid techniques more robust. On the other hand, the estimated time scale of the system can be used to set proper simulation time, which is vital for robust computation and model parameter estimation particularly for steady-state PBE.

In this study, to address these issues, a new approximation technique is proposed to estimate the steady and transient behaviors in the forms of time and length scales for a spatially homogeneous particulate system considering breakage and coalescence. Subsequently, these scales are utilized to form an element-based orthogonal collocation scheme to discretize and solve both transient and steady-state PBE.

2. Mathematical analysis of spatially homogeneous PBE

2.1. Radius-based truncated PBE for dimensionless volume density function

In this study, we consider the population balance equation for a spatially homogeneous particulate system without inflow/outflow. For more ease of derivation, we use the PBE for a radius-based volume density distribution in dimensionless form. This will make working with DSD more convenient. To be able to analyze the problem numerically, the internal domain is truncated to a maximum droplet radius (r_m) which yields the following equation (for detailed derivation the interested reader is referred to the Supplementary material):

$$\frac{\partial \hat{f}_{v,r}(\hat{r},\hat{t})}{\partial \hat{t}} = (t_c r_m)\int_{\hat{r}}^{1} 2g(\hat{r}')\beta_r(\hat{r}',\hat{r})\hat{f}_{v,r}(\hat{r}',\hat{t})\frac{\hat{r}^3}{\hat{r}'^3}d\hat{r}' - t_c g(\hat{r})\hat{f}_{v,r}(\hat{r},\hat{t}) + \left(\frac{t_c}{v_m}\right)\int_0^{\hat{r}/\sqrt[3]{2}} k(\hat{r}',\hat{r}'')\hat{f}_{v,r}(\hat{r}',\hat{t})\hat{f}_v(\hat{r}'',\hat{t})\frac{\hat{r}^5}{\hat{r}'^3\hat{r}''^5}d\hat{r}' - \left(\frac{t_c}{v_m}\right)\hat{f}_{v,r}(\hat{r},\hat{t})\int_0^1 k(\hat{r}',\hat{r})\hat{f}_{v,r}(\hat{r}',\hat{t})\frac{1}{\hat{r}'^3}d\hat{r}' \quad (1)$$

where the terms on the right-hand side of the equation from left to right are breakage birth, breakage death, coalescence birth, coalescence death. $\hat{r}$ is dispersed phase dimensionless droplet radius (r/r_m), $\hat{t}$ is dimensionless time (t/t_c), $\hat{f}_{v,r}(\hat{r},\hat{t})$ is the dimensionless radius-based volume density for droplet radius $\hat{r}$ at time $\hat{t}$, $g(\hat{r})$ is the breakage frequency for droplet radius $\hat{r}$, $\beta_r(\hat{r}',\hat{r})$ is the radius-based daughter distribution of droplet radius $\hat{r}$ resultant from breakage of droplet size $\hat{r}'$, and $k(\hat{r}',\hat{r}'')$ is the rate of coalescence between droplet sizes of $\hat{r}'$ and $\hat{r}'' = (\hat{r}^3 - \hat{r}'^3)^{1/3}$. t_c is the selected characteristic time scale for the system. v_m is the equivalent droplet volume for droplet size equal to r_m. The factor 2 in the breakage birth term appeared as only binary breakage of droplets are considered in this study.

By truncating the domain, the main uncertainty regarding the numerical solution of the PBE appears in the problem. It must be noticed that at this stage, the proper numerical value of r_m is still unknown. Now, in the mentioned PBE framework, the distribution features can be conveniently computed by:

$$N(\hat{t}) = \frac{1}{v_m}\int_0^1 \frac{\hat{f}_{v,r}(\hat{r},\hat{t})}{\hat{r}^3}d\hat{r} \quad (2)$$

$$\phi(\hat{t}) = \int_0^1 \hat{f}_{v,r}(\hat{r},\hat{t})d\hat{r} \quad (3)$$

$$\hat{\mu}_r(\hat{t}) = \frac{\mu_r(\hat{t})}{r_m} = \frac{1}{\phi(\hat{t})}\int_0^1 \hat{f}_{v,r}(\hat{r},\hat{t}).\,\hat{r}.\,d\hat{r} \quad (4)$$

$$\hat{\sigma}_r(\hat{t}) = \frac{\sigma_r(\hat{t})}{r_m} = \left(\frac{1}{\phi(\hat{t})}\int_0^1 (\hat{r}-\hat{\mu}_r)^2 \hat{f}_{v,r}(\hat{r},\hat{t})\,d\hat{r}\right)^{0.5} \tag{5}$$

where N, ϕ, $\hat{\mu}_r$ and $\hat{\sigma}_r$ are the total number of droplets per unit volume, volume fraction, dimensionless average droplet radius, and dimensionless droplet radius standard deviation, respectively.

2.2. A simple kernel with an analytical solution

An analytical solution to PBE subject to simple kernels ($g(r) = sr^3$, $k(r', r) = c$, $\beta_r(r', r) = 3r^2/r'^3$ where s and c are constants) has been proposed by Benjamin and Madras (2003). They solved transient PBE for the mentioned system subject to an initial DSD given by an exponential form. The dimensional analysis of PBE for this system shows that equilibrium distribution can be characterized merely by one dimensionless group (details in the Supplementary material). The analytical solution in the form of dimensionless radius-based volume density, takes the following form (derivation in the Supplementary material).

$$\hat{f}_{v,r}(\hat{r}, t) = \hat{k}_1(t)\hat{r}^5 \exp(-\hat{k}_2(t)\hat{r}^3) \tag{6}$$

where $\hat{k}_1$ and $\hat{k}_2$ are as follows:

$$\hat{k}_1(t) = 4\pi\hat{n}(t)^2 \frac{m_0(0)^2}{m_3} {r_m}^6 \tag{7}$$

$$\hat{k}_2(t) = \hat{n}(t)\frac{m_0(0)}{m_3}{r_m}^3 \tag{8}$$

where $m_0(0)$ is 0th order moment and equivalent to the total number of droplets at initial condition. m_3 is the 3rd order moment and related to the volume fraction of the dispersed phase by $3\phi/(4\pi)$. $\hat{n}(t)$ is also defined as:

$$\hat{n}(t) = \hat{n}(\infty)\left[\frac{1+\hat{n}(\infty)\tanh\left(\hat{n}(\infty)\frac{m_0(0)ct}{2}\right)}{\hat{n}(\infty)+\tanh\left(\hat{n}(\infty)\frac{m_0(0)ct}{2}\right)}\right] \tag{9}$$

$$\hat{n}(\infty) = \left(\frac{2sm_3}{c}\right)^{\frac{1}{2}}\left(\frac{1}{m_0(0)}\right) \tag{10}$$

By setting time in Eqs. 7 and 8 to infinity, equilibrium distribution yields using $\hat{k}_1$ and $\hat{k}_2$ as follows:

$$\hat{k}_1(\infty) = 8\pi\left(\frac{s}{c}{r_m}^6\right) \tag{11}$$

$$\hat{k}_2(\infty) = \left(\frac{8\pi}{3}\right)^{1/2}\left(\frac{1}{\phi}\frac{s}{c}{r_m}^6\right)^{\frac{1}{2}} \tag{12}$$

Eq. 6 describes the dimensionless volume density distribution at a specific time. However, the focus of this study is to propose some simple relations that can approximate the equilibrium and transient behavior of any given kernels. To do that, it is necessary to derive some key features for the distributions. Such features are average droplet radius, standard deviation, peak droplet radius as well as head and tail of the distributions. The mentioned features are presented in the Supplementary material for transient distributions.

2.3. Steady-state analysis of general kernels

As mentioned in the previous section, the whole equilibrium distribution for the simple set of kernels can be characterized by only one dimensionless group of parameters. The mentioned property can also be seen in the main volume-density distribution features at equilibrium condition as follows:

$$\hat{\mu}_r = \frac{4}{9}\left(\frac{3}{8\pi}\right)^{\frac{1}{6}}\Gamma^{-1}(1/3,\,0)M \cong 0.8355M \tag{13}$$

$$\hat{\sigma}_r = \frac{1}{9}\left(\frac{3}{8\pi}\right)^{\frac{1}{6}}\left(90\Gamma^{-1}\left(\frac{2}{3},\,0\right) - 16\Gamma^{-1}\left(\frac{1}{3},\,0\right)^2\right)^{0.5} M \cong 0.2069M \tag{14}$$

$$\hat{r}_{peak} = \left(\frac{25}{24\pi}\right)^{\frac{1}{6}} M \cong 0.8319M \tag{15}$$

where the dimensionless term M is defined as below:

$$M = \left(\frac{\phi}{\frac{s}{c}{r_m}^6}\right)^{\frac{1}{6}} \tag{16}$$

Accordingly, the significant property of these simple kernels is that all the key features of the equilibrium distribution have a linear relation to the dimensionless number M. Eqs. 13–15 provides the exact values for the equilibrium behavior of the simple kernels. However, it is generally possible to extend this approach to approximate these behaviors for any other kernels of interest. Such a task requires the extraction of some values from the kernel function as representative values for c and s for the equilibrium distribution. In the system with the analytical solution, the values of c and s are constants while generally they can have functionality of the droplet size. For that, we propose averaging these values weighted by the equilibrium volume density distribution over the internal domain as follows:

$$s_{est}(\infty) = \frac{1}{\phi}\int_0^\infty \hat{f}_{v,r}(\hat{r},\infty)\frac{g(r)}{r^3}d\hat{r} \tag{17}$$

$$c_{est}(\infty) = \frac{1}{\phi^2}\int_0^\infty\int_0^\infty \hat{f}_{v,r}(\hat{r}',\infty)\hat{f}_{v,r}(\hat{r},\infty)k(r', r)\,d\hat{r}'d\hat{r} \tag{18}$$

The above terms are computationally expensive as the single, and especially double integrals are expensive to compute numerically; additionally, they contain the equilibrium distribution ($\hat{f}_{v,r}(\hat{r}',\infty)$) that is still unknown at this point, which we aim to estimate. To make the math more manageable and to avoid the difficulties of evaluating of the integral, we assume the whole distribution is concentrated at the average droplet radius. Mathematically, this can be handled using the Dirac delta function at the average points as $\hat{f}_{v,r}(\hat{r},\infty) = \phi\delta(\hat{r}-\hat{\mu}_r(\infty))$. It is worth mentioning that other forms of functions for $\hat{f}_{v,r}(\hat{r},\infty)$ can still be assumed (e.g. exponential and log-normal); however, such an assumption would need directly solving the above integrals. In any case, the first thing to do is to start from $\hat{\mu}_r(\infty)$ as an initial guess and solve iteratively.

The mentioned Dirac delta function assumption significantly simplifies the Eqs. 17 and 18 to the following ones:

$$s_{est}(\infty) = \frac{g(\mu_r(\infty))}{\mu_r(\infty)^3} \tag{19}$$

$$c_{est}(\infty) = k(\mu_r(\infty), \mu_r(\infty)) \tag{20}$$

Now, the approximated representative values have only the dependency of the average droplet radius of equilibrium distribution. At the same time, according to Eq. 13, the average droplet radius of equilibrium distribution has the

dependency of dimensionless value M, which can be calculated by knowing the representative values $s_{est}(\infty)$, $c_{est}(\infty)$. In other words, Eqs. 13, 19, and 20 forms a nonlinear system of equations which can be solved by any numerical technique to yield the values for $s_{est}(\infty)$, $c_{est}(\infty)$, and $\hat{\mu}_r(\infty)$. For that purpose, an illustrating iterative approach is proposed and demonstrated in the Supplementary material section.

By knowing the numerical values for $s_{est}(\infty)$, $c_{est}(\infty)$, it is now possible to approximate the equilibrium distribution using Eq. 6. Consequently, the internal domain bound can be simply specified by calculating the head and tail of the equilibrium distribution. One possible way to define head and tail is by obtaining the droplet radius sizes at which the smaller droplet sizes yield a specific value of volume fraction (typically 1 % and 99 % for the tail and head, respectively). This can mathematically be defined as follows:

$$\phi_x = x\phi = \int_0^{\hat{r}_x} \hat{f}_{v,r}(\hat{r}, \infty)\, d\hat{r} \tag{21}$$

where ϕ_x is the volume fraction of interest and can have a value between 0 and ϕ and the typical values would be 0.01ϕ and 0.99ϕ for tail and head of the distribution, respectively. By using this definition (Eq. 21) and substituting $\hat{f}_{v,r}$ using Eq. 6, the following equation is obtained.

$$\phi_x = x\phi = \phi - \frac{k_1(\infty)exp(-k_2(\infty)\hat{r}_x^3)(k_2(\infty)\hat{r}_x^3 + 1)}{3k_2(\infty)^2} \tag{22}$$

Rearranging Eq. 22, forms the final equation to calculate the head and tail of the equilibrium distribution as follows:

$$\left(\left(\frac{8\pi}{3}\right)^{\frac{1}{2}}\left(\frac{\hat{r}_x}{M}\right)^3 + 1\right)\exp\left(-\left(\frac{8\pi}{3}\right)^{\frac{1}{2}}\left(\frac{\hat{r}_x}{M}\right)^3\right) - (1 - x) = 0 \tag{23}$$

Eq. 23 is a nonlinear equation and can be solved numerically for $\hat{r}_x$ for a target value of x. Consequently, for steady-state PBE, the truncation point for the internal domain can be specified as head plus a safety margin. For transient PBE, this value should be selected considering the initial distribution and approximated equilibrium distribution simultaneously. This issue is explained with more details in Section 3.

2.4. *Transient analysis of general kernels*

The characteristic time scale for a transient system can be defined as the transient time required for the system to evolve from the initial condition to a particular state closer to the equilibrium state. For our specific case, we approximate this value according to the transient behavior of the average droplet radius. That is, the time required for the average droplet radius to move a fraction of the distance between initial and equilibrium average radii. This can mathematically be expressed by:

$$\hat{\mu}_r(t_x) = x[\hat{\mu}_r(\infty) - \hat{\mu}_r(0)] + \hat{\mu}_r(0) \tag{24}$$

The value of x in Eq. 24 can be selected between 0 and 1. In this study, we consider x as 0.9. This choice was based on our observation (the cases that we studied in this work) that $3 \times t_{0.9}$ can practically be considered as the required time to reach the equilibrium state. However, it might not be appropriate for other kernels, and the proper choice of these values (x and the factor of the time scale) can be evaluated and possibly slightly modified for a specific system under study to achieve an equilibrium state.

For the simple kernels, Eq. 24 can be solved for t_x to yield exact values of transient time; nonetheless, this equation cannot be directly extended to other kernels as the representative values $s_{est}(t)$, $c_{est}(t)$ are not generally constant, and their time functionalities needs to be considered. To overcome this, we propose an approximation of the transient time by integrating the rate of change in the average droplet radius. Mathematically, the problem can be outlined as:

$$t_x = \int_{\hat{\mu}_r(0)}^{\hat{\mu}_r(t_x)} \frac{1}{\frac{d\hat{\mu}_r}{dt}(\hat{\mu}_r)} d\hat{\mu}_r \tag{25}$$

The term $d\hat{\mu}_r/dt(\hat{\mu}_r)$ is the rate of change in the average droplet radius of dimensionless volume density distribution at any given $\hat{\mu}_r$ and has the dimension equal to the inverse of time. A useful property of the analytical solution for the simple kernels is that initial form of the distribution (Eq. 6) is always preserved. Taking advantage of it, we can calculate $d\hat{\mu}_r/dt(\hat{\mu}_r)$ by just setting time to zero provided that we modify the value for the total number of droplets per unit volume, m_0 according to the pertinent $\hat{\mu}_r$. Based on the derived equation for the transient average radius in the appendix section, this term can be mathematically obtained for the simple kernels as follows:

$$\frac{d\hat{\mu}_r}{dt}(\hat{\mu}_r) = -\frac{0.7386}{3}\frac{\phi^{\frac{1}{3}}}{r_m \hat{n}(0)^{\frac{4}{3}} m_0^{\frac{1}{3}}}\frac{d\hat{n}(0)}{dt} \tag{26}$$

where $\hat{n}(0)$ is simply equal to one and $d\hat{n}/dt(0)$ can be calculated as:

$$\frac{d\hat{n}(0)}{dt} = \frac{m_0 c}{2}(\hat{n}^2(\infty) - 1) \tag{27}$$

By substitution, Eq. 26 takes the following form:

$$\frac{d\hat{\mu}_r}{dt}(\hat{\mu}_r) = -\frac{0.7386}{3}\frac{\phi^{\frac{1}{3}}}{r_m}\frac{m_0^{\frac{2}{3}} c}{2}\left(\frac{3}{2\pi}\frac{s\phi}{c m_0^2} - 1\right) \tag{28}$$

As also mentioned, m_0 in Eq. 28 should be corrected by taking the change in the initial number of droplets into account as the distribution evolves. This value can be calculated by Eq. 2. as follows:

$$m_0 = \frac{1}{v_m}\int_0^1 \frac{\hat{f}_{v,r}(\hat{r}, t)}{\hat{r}^3} d\hat{r} \tag{29}$$

Similarly, to simplify the equation and rectify the need to calculate the integral numerically, the whole distribution is assumed to be concentrated at the average radius, $\hat{f}_{v,r}(\hat{r}, t) = \phi\delta(\hat{r} - \hat{\mu}_r)$. By that simplification, number of droplets per unit volume at every $\hat{\mu}_r$ is given by:

$$m_0 \approx \frac{1}{v_m}\int_0^1 \frac{\phi\delta(\hat{r} - \hat{\mu}_r)}{\hat{r}^3} d\hat{r} = \frac{\phi}{v_m \hat{\mu}_r{}^3} \tag{30}$$

By plugging Eq. 30 in 28, it yields:

$$\frac{d\hat{\mu}_r}{dt}(\hat{\mu}_r) \approx 0.0474\frac{\phi}{r_m{}^3}\frac{c(\hat{\mu}_r)}{\hat{\mu}_r{}^2}\left(1 - 8.3776\frac{r_m{}^6}{\phi}\frac{s(\hat{\mu}_r)\hat{\mu}_r{}^6}{c(\hat{\mu}_r)}\right) \tag{31}$$

Eq. 31 describes the key dependencies for the rate of change in the average droplet radius for a dimensionless volume density distribution. However, due to the simplifying assumptions made, Eq. 31 cannot properly predict the time scales for the simple kernel. To remedy this, we reevaluate the constant numerical values in Eq. 31 as follows.

$$\frac{d\hat{\mu}_r}{dt}(\hat{\mu}_r) \approx C_1 \frac{\phi}{r_m{}^3} \frac{c(\hat{\mu}_r)}{\hat{\mu}_r{}^2} \left(1 - C_2 \frac{r_m{}^6}{\phi} \frac{s(\hat{\mu}_r)\hat{\mu}_r{}^6}{c(\hat{\mu}_r)}\right) \tag{32}$$

We can make use of the fact that $d\hat{\mu}_r/dt(0)$ should be equal to zero at equilibrium distribution, i.e., $\hat{\mu}_r = 0.8355M$. This constraint gives the exact value of C_2 equal to 2.94. Additionally, the numerical value of C_1 is tuned for the simple kernels with the available analytical solution using several test cases by changing different numerical values for ϕ, s, and c. Adjusting C_1 was performed by minimization of the average absolute relative deviation (AARD) of total studied cases using MATLAB unconstrained nonlinear optimization functionality (fminunc). The deviation was the calculated between predicted time scale ($t_{0.9}$) by Eq. 32 and that obtained from numerical computation. The final equation takes the following form.

$$\frac{d\hat{\mu}_r}{dt}(\hat{\mu}_r) \approx 0.067 \frac{\phi}{r_m{}^3} \frac{c(\hat{\mu}_r)}{\hat{\mu}_r{}^2} \left(1 - 2.94 \frac{r_m{}^6}{\phi} \frac{\hat{s}(\hat{\mu}_r)\hat{\mu}_r{}^6}{\hat{c}(\hat{\mu}_r)}\right) \tag{33}$$

Having derived the expression of $d\hat{\mu}_r/dt(\hat{\mu}_r)$ for simple kernel, the next step is to extend it to generalized kernels which can be done by replacing c and s terms with estimated values similar to the previous section as follows:

$$\frac{d\hat{\mu}_r}{dt}(\hat{\mu}_r) \approx 0.067 \frac{\phi}{r_m{}^3} \frac{c_{est}(\hat{\mu}_r)}{\hat{\mu}_r{}^2} \left(1 - 2.94 \frac{r_m{}^6}{\phi} \frac{s_{est}(\hat{\mu}_r)\hat{\mu}_r{}^6}{c_{est}(\hat{\mu}_r)}\right) \tag{34}$$

where s_{est} and c_{est} can be estimated by:

$$s_{est}(\hat{\mu}_r) = \frac{g(\mu_r)}{\mu_r{}^3} \tag{35}$$

$$c_{est}(\hat{\mu}_r) = k(\mu_r, \mu_r) \tag{36}$$

Moreover, Eq. 34 can also be rearranged based of the dimensionless group M as follows:

$$\frac{d\hat{\mu}_r}{dt}(\hat{\mu}_r) \approx 0.067 \frac{\phi}{r_m{}^3} \frac{c_{est}(\hat{\mu}_r)}{\hat{\mu}_r{}^2} \left(1 - 2.94 \frac{\hat{\mu}_r{}^6}{M^6}\right) \tag{37}$$

According to the derived expression, when both the breakage and coalescence are present in the system, the rate of the change in the average radius for a dimensionless volume density is proportional to the volume fraction of dispersed phase, the average value of the coalescence rate at that state, and inversely proportional to the square of distribution average radius. This rate is also influenced by the term $(1 - 2.94\hat{\mu}_r{}^6/M^6)$ which determines how remote the system is from equilibrium state. This term can also predict the direction that the distribution is likely to evolve as:

- When positive (equivalent to $\hat{\mu}_r > 0.8355M$), the distribution evolves toward larger droplet sizes.
- When negative (equivalent to $\hat{\mu}_r < 0.8355M$), the distribution evolves toward smaller droplet sizes.
- When zero (equivalent to $\hat{\mu}_r = 0.8355M$), the system is at equilibrium state.

Furthermore, the following similar dependencies are deducted for the systems with either pure breakage or coalescence as follows:

- For a system with pure coalescence, the rate of the change in the average radius for a dimensionless volume density is only proportional to the volume fraction of dispersed phase, and the average value of the coalescence rate at that state and inversely proportional to the square of distribution average radius.
- For a system with pure breakage, the rate of the change in the average radius for a dimensionless volume density is only proportional to both average breakage frequency at that state and distribution average radius.

Now, having the explicit expression for $d\hat{\mu}_r/dt(\hat{\mu}_r)$, the time scale for the system can be conveniently calculated according to Eq. 25.

3. Numerical analysis of the PBE

The orthogonal collocation method (Villadsen and Michelsen, 1978) is used to discretize the internal domain in an element-based form. The primary strategy for generating the grid is to use the least number of elements while keeping the order of the polynomials high enough to have proper error decaying properties. However, it is still helpful to specify a certain number of elements to make the technique more flexible. Collocation points are selected according to the roots of the Jacobi polynomials, and quadrature weights are calculated accordingly. The monotone piecewise cubic Hermite interpolation technique was used (Fritsch and Carlson, 1980) to map the grid points to collocation points (which is essential to calculate the integrals in the coalescence and breakage birth rates). The orthogonal collocation points (Gauss-Radau and Gauss-Lobatto) are not uniformly distributed over an element but more concentrated closer to the edges. As a result, in the case of applying the full spectral technique, the described interpolation technique would not be accurate enough. Additionally, a full spectral technique cannot numerically capture narrow DSDs. The element-based grid can be advantageous in addressing these issues.

For a steady-state problem, four elements are used and selected according to specific locations of the estimated equilibrium distribution. This issue is graphically demonstrated in Fig. 1. Accordingly, the first element is from zero to the tail of the distribution; the second element from the tail to the average radius of the distribution; the third element is from the average radius to the head of the distribution, and the last element is from the head of the distribution to the truncation point (200% of the head).

For transient PBM, a 5-element grid is generated considering two distributions, namely, initial distribution and estimated equilibrium distribution. The element boundaries are selected as:

- zero
- minimum of tails of both distributions;
- average radius of initial distribution;
- average radius of estimated equilibrium distribution;
- maximum of heads of both distributions;
- truncation point (200 % of the maximum of heads of both distributions)

equilibrium distribution can be either right, left, or overlapping with the initial distribution. Therefore, the locations of the boundary elements need to be specified by sorting these boundary points. Moreover, for severe cases where initial and equilibrium distributions are distant from each other, it is wise to add more than one element between the average radii of the two distributions or alternatively more collocation points for this region. Comparison of the DSD

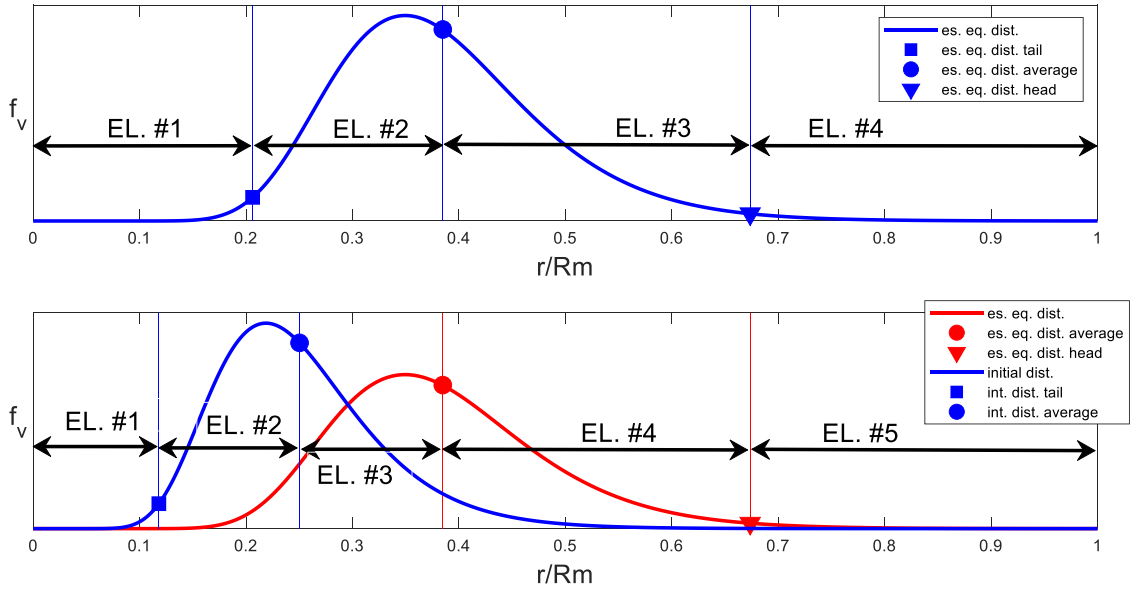

Fig. 1 – Elements used for numerical computation; top: steady-state PBE; bottom: transient PBE.

standard deviation (which gives an idea about the width of the distribution) with this range can also be an excellent criterion for determining the proper number of elements. In this work, for all the studied cases, only one element is used for this region. Overall, four different grid sizes were evaluated with number of collocation points per element equal to 5, 10, 15 and 20 in Section 4.3.

Discretization of the steady-state problem forms a nonlinear set of equations, which were solved iteratively (detail in the Supplementary material). For the transient case, the discretized system of ODEs was integrated using the adaptive Gear's backward differentiation scheme. The iteration and time integration tolerances were both set to 10^{-6}. The simulation time was also set as $3 \times t_{0.9}$ to calculate the equilibrium distribution.

4. Results and discussion

To evaluate the technique, two sets of kernels for liquid-liquid dispersions are used. The kernels are relevant to turbulent systems. The kernel relations together with their parameters are summarized in Table 1.

The breakage and coalescence models show dependencies to system physiochemical properties, namely, phases' densities and interfacial tension as well as hydrodynamic properties like turbulence energy dissipation rates.

Table 1 – Kernels used for case studies.

Kernels #1	coalescence rate	$k(r',r) = \omega(r',r)\psi_E(r',r) \quad \omega(r',r) = k_{c1}2^{\left(\frac{1}{3}\right)}\varepsilon^{\left(\frac{1}{3}\right)}(r'+r)^2(r'^{(2/3)}+r^{(2/3)})^{\left(\frac{1}{2}\right)} \quad \psi_E(r',r) = \exp\left(-k_{c2}2^{\left(-\frac{1}{6}\right)}\frac{\rho_c^{\left(\frac{1}{2}\right)}\varepsilon^{\left(\frac{1}{3}\right)}}{\tau^{\left(\frac{1}{2}\right)}}\left(\frac{1}{r'}+\frac{1}{r}\right)^{\left(-\frac{5}{6}\right)}\right)$	$k_{c1} = 0.001 \quad k_{c2} = 1$	collision efficiency (Prince and Blanch, 1990), coalescence efficiency (Chesters, 1991)
	breakage frequency	$g(r) = k_{b1}\frac{\varepsilon^{\left(\frac{1}{3}\right)}}{2^{\left(\frac{2}{3}\right)}}\left(\frac{\rho_d}{\rho_c}\right)^{\left(\frac{1}{2}\right)}\frac{1}{r^{\left(\frac{2}{3}\right)}} \quad \exp\left(-k_{b1}\frac{\tau}{2^{\left(\frac{5}{3}\right)}\rho_d\varepsilon^{\left(\frac{2}{3}\right)}}\frac{1}{r^{\left(\frac{5}{3}\right)}}\right)$	$k_{b1} = 1 \quad k_{b1} = 1$	(Vankova et al., 2007)
	daughter distribution	$\beta_r(r',r) = 7.2\frac{r^2}{r'^3}\exp\left(-4.5\frac{(2r^3-r'^3)^2}{r'^6}\right)$		(Coulaloglou and Tavlarides, 1977)
Kernels #2	coalescence rate	$k(r',r) = \omega(r',r)\psi_E(r',r) \quad \omega(r',r) = k_{c1}2^{\left(\frac{7}{3}\right)}\varepsilon^{\left(\frac{1}{3}\right)}(r'+r)^{\left(\frac{7}{3}\right)} \quad \psi_E(r',r) = \exp\left(-k_{c2}2^{\left(-\frac{1}{6}\right)}\frac{\rho_c^{\left(\frac{1}{2}\right)}\varepsilon^{\left(\frac{1}{3}\right)}}{\tau^{\left(\frac{1}{2}\right)}}\left(\frac{1}{r'}+\frac{1}{r}\right)^{\left(-\frac{5}{6}\right)}\right)$	$k_{c1} = 0.1 \quad k_{c2} = 1$	(Chesters, 1991)
	breakage frequency	$g(r) = 2^{\left(-\frac{2}{3}\right)}k_{b1}\frac{\varepsilon^{\left(\frac{1}{3}\right)}}{r^{\left(\frac{2}{3}\right)}}\left(erfc(w^{0.5}) + \frac{2}{\pi^{0.5}}w^{0.5}\exp(-w)\right) \quad w_e = 2^{\left(\frac{8}{3}\right)}\frac{\rho_c\varepsilon^{\left(\frac{2}{3}\right)}}{\tau}r^{\left(\frac{5}{3}\right)} \quad w = 1.5\frac{k_{b2}}{w_e}$	$k_{b1} = 1 \quad k_{b2} = 0.5$	(Eskin et al., 2017)
	daughter distribution	$\beta_r(r',r) = 90\frac{r^2}{r'^3}\left(\frac{r}{r'}\right)^6\left(1-\left(\frac{r}{r'}\right)^3\right)^2$		(Hsia and Tavlarides, 1983)

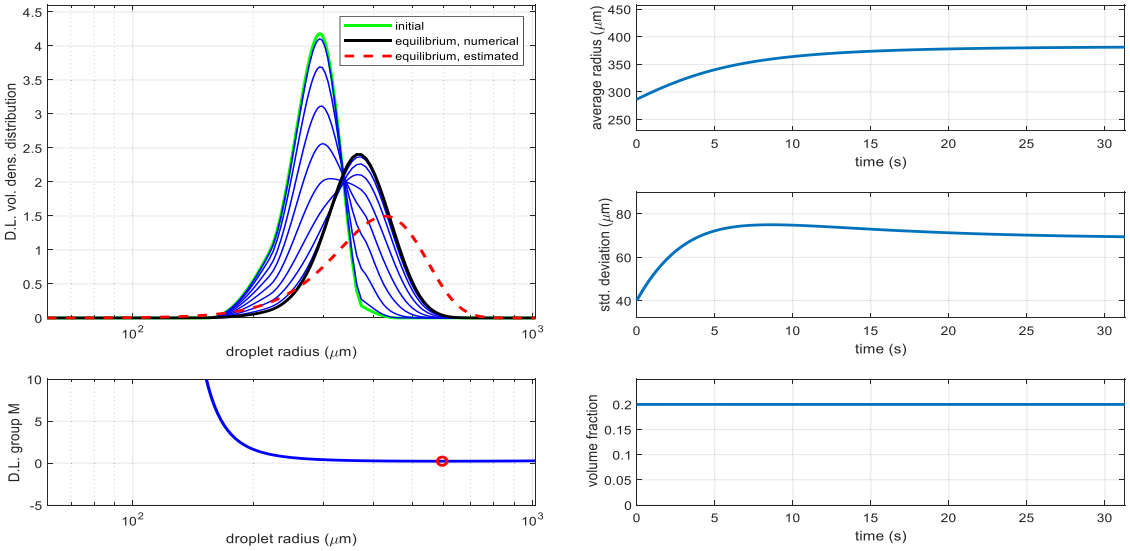

Fig. 2 – Comparison of estimated equilibrium distribution with numerical results for kernels #1, volume fraction = 0.2 and turbulence dissipation rate = 0.5 m^2s^{-3}**.**

Another influential parameter for the system behavior is dispersed phase volume fraction, which can significantly affect the system equilibrium and transient behavior. In this study, the two most influential parameters, namely, dispersed phase volume fraction as well as turbulence energy dissipation rate, are studied. The studied system is a typical water-in-oil emulsion, and the physiochemical parameters were kept constants for all the studied cases with numerical values as follows: dispersed phase density= 1000 kg/m^3, continuous phase density= 900 kg/m^3, interfacial surface tension: 30 mN/m.

The dynamic simulation results for the two extreme cases are depicted in the Figs. 2 and 3 for both sets of kernels. For all the simulations, the same initial distribution with an average point at 285 μm and standard deviation of 40 μm were used. The approximation technique is evaluated by comparing it with the results of the element-based orthogonal collocation technique with 20 collocation points per element (5-element fine grid for transient problem). It is worth noting that the estimated equilibrium distributions (dashed red curves) in the following figures are not the final result of the proposed technique but a starting point to perform more efficient computations for the PBE.

In Figs. 2 and 3, the evolution of the distribution is plotted from initial to equilibrium distribution and compared to the estimated equilibrium distribution. The estimated distributions almost always show tilting of the distribution peaks toward the left. It is worth noting that the estimated equilibrium distribution is inexact and deviates slightly from the simulated equilibrium distribution for Kernels #1 and #2. Nevertheless, in the case of a simple kernel, the estimated and simulated equilibrium distributions would be identical. This matter has been explained in more detail and used to verify the numerical technique in Section 4.3. Dimensionless

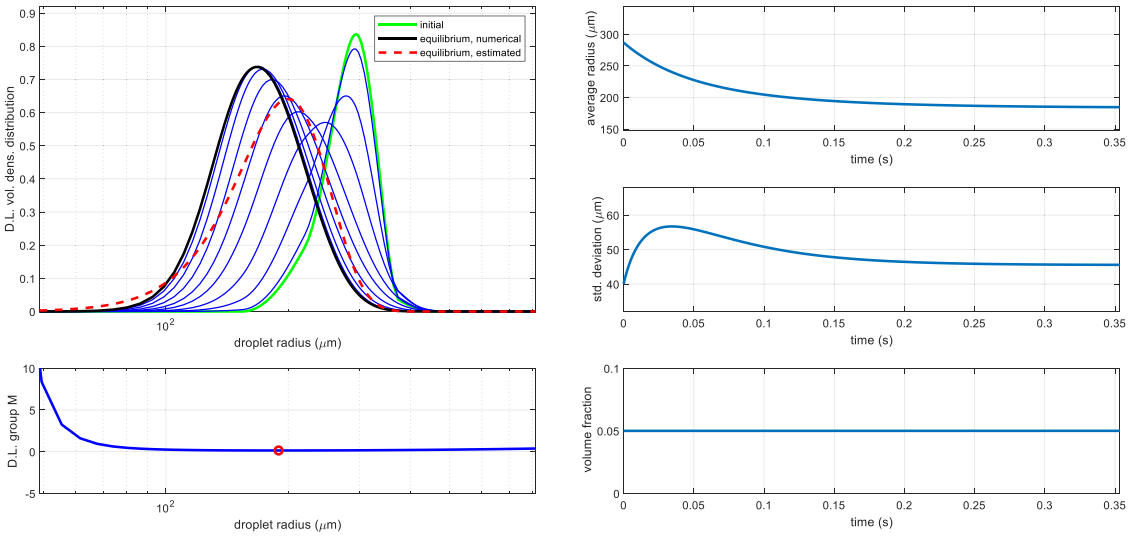

Fig. 3 – Comparison of estimated equilibrium distribution with numerical results for kernels #2, volume fraction = 0.05 and turbulence dissipation rate = 2 m^2s^{-3}**.**

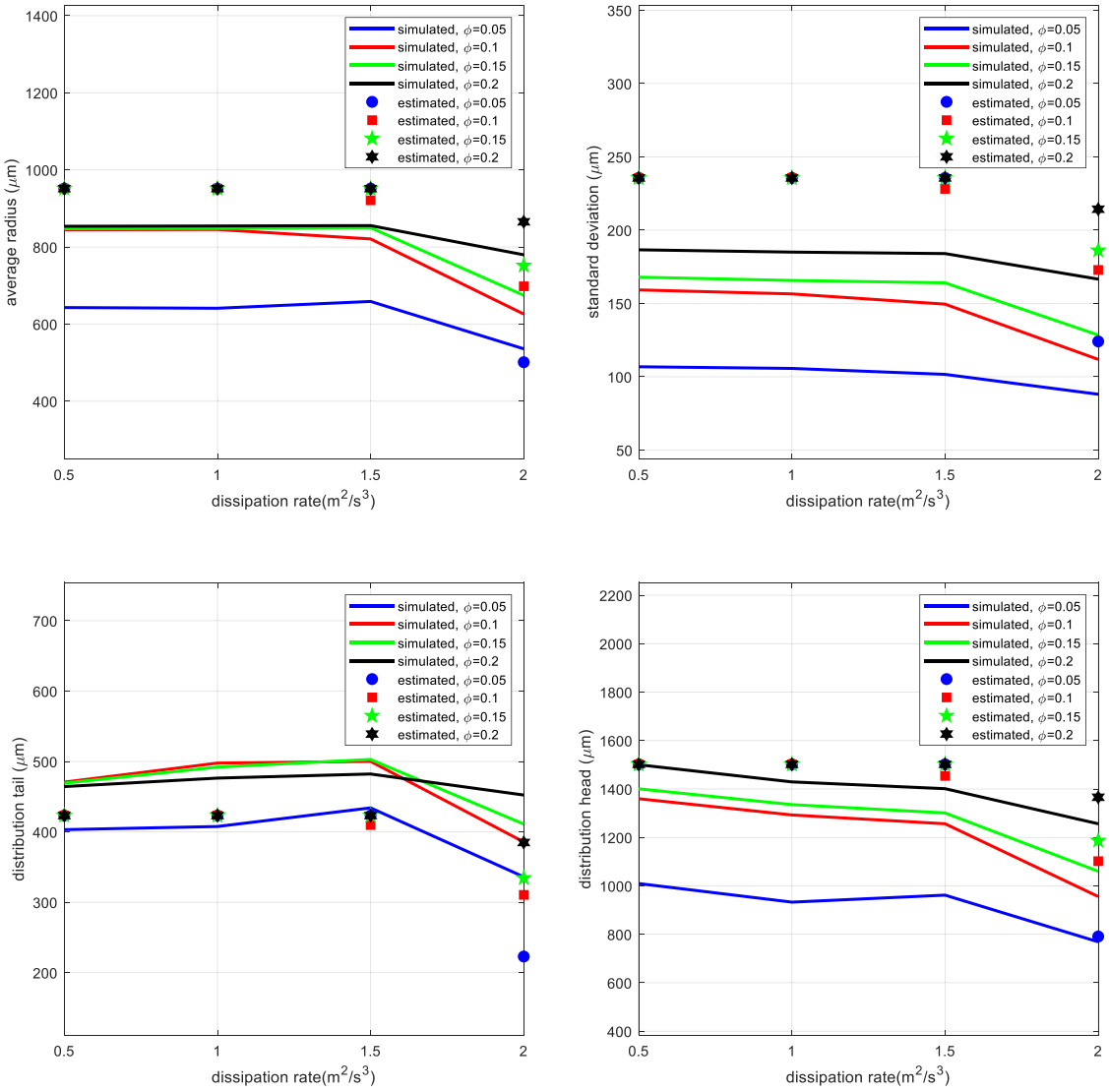

Fig. 4 – Comparison of estimated length scales with simulation results, kernels #1.

group *M* versus droplet size is also depicted in Figs. 2 and 3. This curve shows a minimum commonly close to the estimated average droplet radius.

4.1. *Approximated equilibrium length scales*

The approximated equilibrium length scales are depicted in Figs. 4 and 5 for kernels #1 and #2.

The technique provides less accurate estimations for extreme conditions with low volume fractions for the case of kernels #1. However, for the other more moderate conditions, the deviation is typically less than 20 % for heads, tails, and averages. Here, the tail is overpredicted while the head is underpredicted. Although it is not satisfactory to be used directly to analyze the system, this still suffices for generating element-based grids. Another important issue is the truncation point. Based on the mentioned results, a 100 % safety margin over the head seems a reasonable choice for truncation of the internal domain. Moreover, all the approximated length scales follow the same trend as that of the numerical simulation. The average droplet size for more moderate cases shows a deviation of around 12 %, while the approximation results for the standard deviation are not as satisfactory, having an average deviation of approximately 58 %.

Overall, the results for kernel #2 show much better agreement between the estimated and simulated length scales. Like the previous case, the estimated standard deviation shows the least agreement with an average deviation of 14 % ranging from 8 % for lower volume fractions to 25 % for higher volume fraction values. The average droplet is slightly overpredicted, with an average deviation of around 7 %. The distribution tail is well estimated with an average deviation of around 5 %. However, the deviation for the head ranges from 2 % for low volume fractions to about 20 % for high volume fractions. The estimated length scales

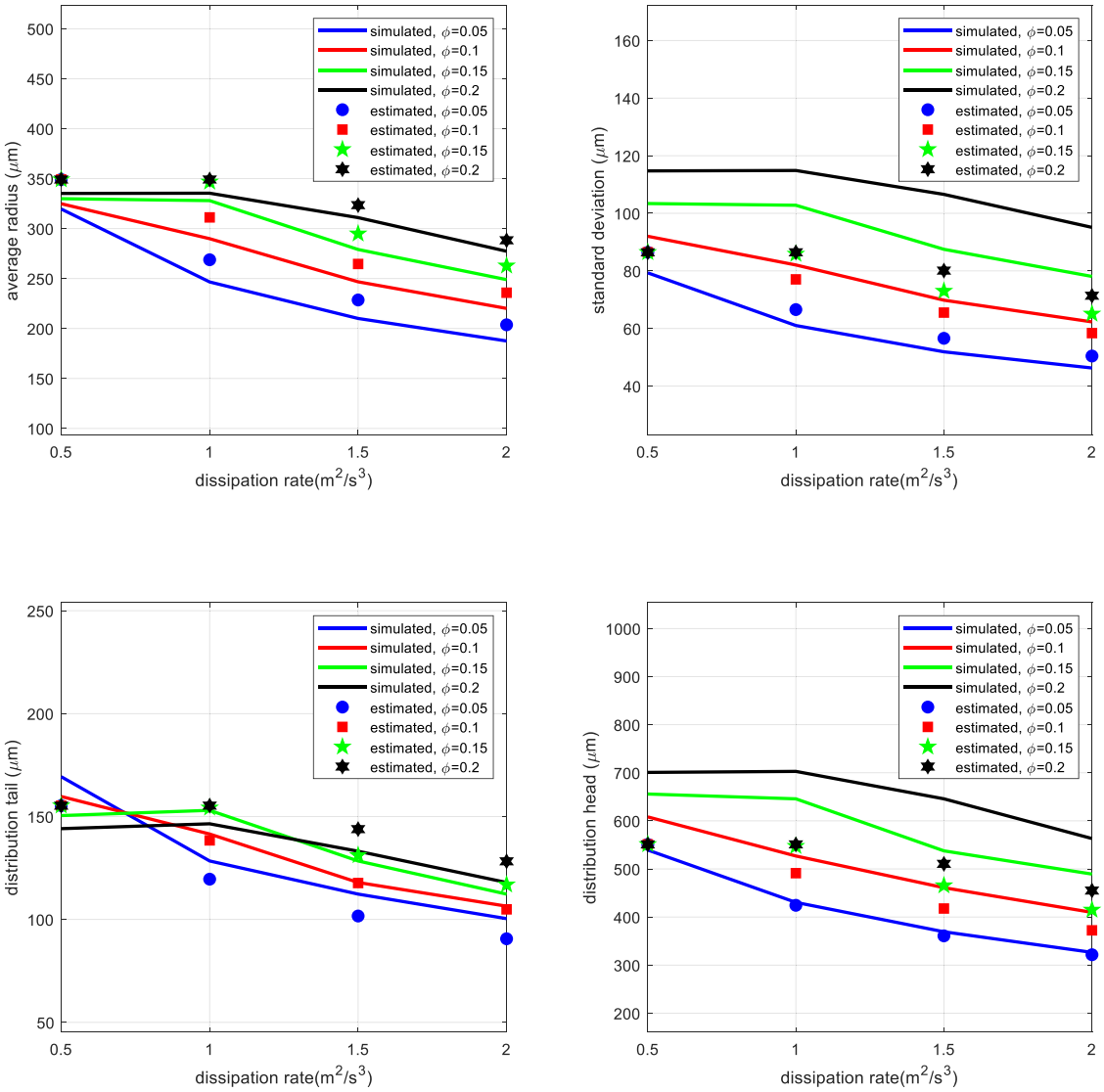

Fig. 5 – Comparison of estimated length scales with simulation results, kernels #2.

completely follow the trend of the simulated length scales. Same as Kernel #1, the results support the 100 % safety margin value over the estimated head for the truncation of the internal domain.

4.2. *Approximated transient time scale*

The estimated timescales based on the $t_{0.9}$ are compared with the simulation results in Fig. 6 for both sets of kernels.

According to Fig. 6, for kernel #1, the deviation for cases with initial and equilibrium distributions distant from each other is typically less than 30 %. However, the prediction accuracy can be influenced in cases with the initial and equilibrium distributions very close, with a deviation as high as 100 %. Similarly, for kernel #2, this deviation for most cases is less than 40%, while for severe cases, with close initial and equilibrium distributions can be as high as 150%. The mentioned issue makes direct usage of the estimated time scales limited. However, technique results can still be used for consequent cumbersome numerical computation by applying a safety margin. Practically, after a time equal to $3 \times t_{0.9}$, the system can be assumed in its equilibrium state. This value ($3 \times t_{0.9}$) provides an excellent choice to terminate the time integration for cases where the equilibrium distribution is desired.

4.3. *Evaluation of the numerical technique*

In this section, the element-based numerical grids are evaluated. The numerical scheme used for the transient PBE is verified versus the available analytical solution for the simple kernel (Benjamin and Madras, 2003) in Fig. 7. This figure has considered two different cases with various values for volume fraction and kernel constants. The grid with 20 collocation points per element perfectly agrees with the analytical solution. In contrast, similar cases with 10 collocation points indicate a slight deviation from the analytical solution.

Weighted residue methods (including orthogonal collocation technique), contrary to a method of classes (Kumar

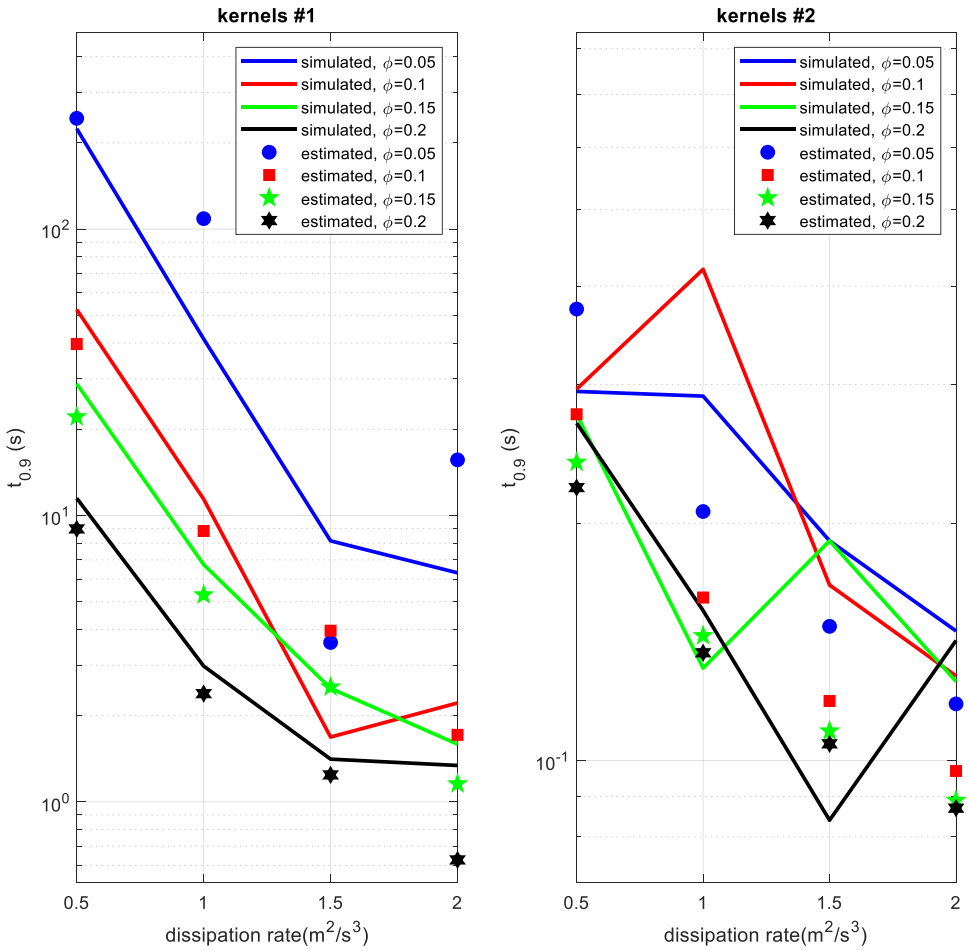

Fig. 6 – Comparison of estimated time scales ($t_{0.9}$) with simulation results.

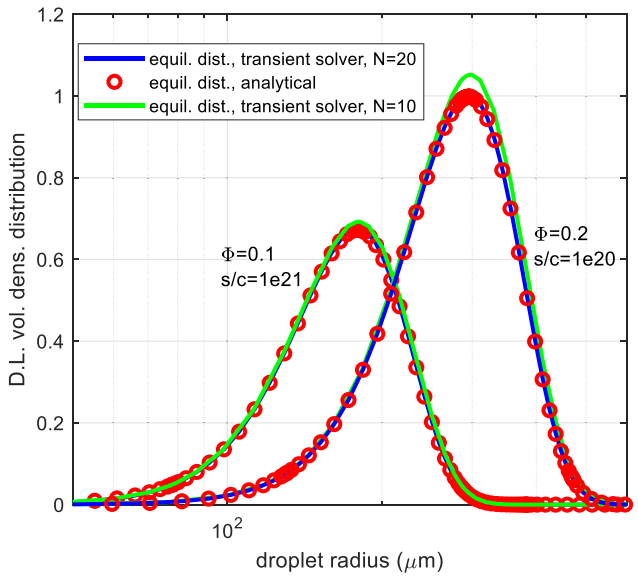

Fig. 7 – Comparison of the calculated equilibrium distribution using various grid sizes with the analytical solution.

and Ramkrishna, 1996a,b) and finite volume method (Filbet and Laurençot, 2004) are not a conservative, meaning that the moment properties like volume fraction are not conserved. For our current problem, the volume fraction is an excellent criterion to check the accuracy of the solution as it should be constant, and the deviation from it reveals the overall imbalance in the numerical solution. Hence, verifying the different grid sizes has been achieved using the deviation of the equilibrium volume fraction from its correct value. Both steady-state and transient solvers were evaluated for different cases using kernel #2 as well as the transient solver for the simple kernel. The results are presented in Table 2.

From Table 2, the numerical grid with 20 collocation points per element for the transient PBE can accurately predict the equilibrium distribution with a numerical imbalance close to a fraction of a percent. Similar grids with 15 collocation points can still provide an acceptable solution for a transient problem. However, by decreasing the number of collocation points to less than 10 per element, the accuracy of the solution drastically drops. The iterative scheme for steady-state PBE does not provide sufficient accuracy for the equilibrium distribution. Specifically, it seems that this iteration solution technique for PBE possesses some intrinsic errors that do not eliminate by refining the mesh. Hence, this

Table 2 – Percentage of the volume fraction deviation.

Studied cases		Collocation points per element			
		5	10	15	20
Kernel #2, transient solver	$\phi = 0.1, \varepsilon = 1$	12.03	1.73	0.33	0.08
	$\phi = 0.1, \varepsilon = 2$	5.10	1.06	0.15	0.02
	$\phi = 0.2, \varepsilon = 1$	20.53	2.59	0.47	0.04
	$\phi = 0.2, \varepsilon = 2$	17.71	1.71	0.22	0.07
Kernel #2, steady-state solver	$\phi = 0.1, \varepsilon = 1$	28.16	15.20	14.91	14.86
	$\phi = 0.1, \varepsilon = 2$	52.41	21.99	19.12	18.43
	$\phi = 0.2, \varepsilon = 1$	39.53	-13.79	-11.43	-11.49
	$\phi = 0.2, \varepsilon = 2$	31.62	17.13	16.47	15.43
Simple Kernel, transient solver	$\phi = 0.1$, s/c = 10^{20}	84.60	6.02	1.12	0.33
	$\phi = 0.1$, s/c = 10^{21}	55.87	3.55	0.66	0.48
	$\phi = 0.2$, s/c = 10^{20}	93.70	6.65	0.72	0.33
	$\phi = 0.2$, s/c = 10^{21}	60.43	3.71	2.23	0.85

Table 3 – Percentage of the decrease in the computation time.

Turbulence dissipation rate (m^2/s^3)	Volume fraction			
	0.05	0.10	0.15	0.20
0.5	67.8	43.5	45.9	57.9
1	56.1	61.3	59.2	65.0
1.5	65.2	64.8	59.6	63.4
2	62.8	68.1	63.7	59.9

technique is not recommended for calculating the equilibrium distribution. Alternatively, a transient solution from the initial distribution as the estimated equilibrium distribution is recommended. The mentioned approach can significantly decrease the computational time required for the solution of the steady-state PBE. The percentage of reduction in the computational time obtained by this technique is summarized in Table 3 for various studied cases using kernel #2. The values are calculated by comparing the computation times of the cases with the initial conditions the same as that in Fig. 3 and the estimated equilibrium distribution. The final simulation time was set as $3 \times t_{0.9}$ with $t_{0.9}$ calculated using the case with the initial condition depicted in Fig. 3. The same absolute final simulation time was also used for the counterpart cases with the initial condition as estimated equilibrium distribution.

Accordingly, this approach has decreased the required computational time by around 40–70%. It must be noted that the decrease in the computation time can be enormously influenced by the distance between the initial and equilibrium distributions. For cases with higher distances, one can expect better improvement in computation efficiency.

5. Conclusion

Based on extrapolating the available analytical solution for the spatially homogeneous PBE with simple breakage and coalescence kernels, a new approach was developed to estimate the equilibrium and transient properties of the problem in the form of the length and time scales of the system. Furthermore, this approach was generalized to any generalized form of breakage and coalescence relations.

All the approximated equilibrium distribution properties have a linear relation with respect to a dimensionless group. In other words, the equilibrium distribution of the system is mainly governed by this dimensionless group. This group shows dependency only on the breakage and coalescence kernels as well as the volume fraction of the dispersed phase.

Similarly, the derived relation for the transient time of the system only shows simple explicit relation concerning kernels and volume fraction and influenced by a term which determines how remote the system is from equilibrium state. This term can predict the direction that the distribution is likely to evolve.

The derived relations for time and length scales were compared with the numerical results of the orthogonal collocation method. The test cases were selected according to two available sets of kernels used for liquid-liquid dispersion. The most influential system parameters were studied, namely, turbulence dissipation rate and volume fraction. Overall, the approximation technique provides satisfactory preliminary information about the time and length scales of the system for the purpose of numerical grid generation and numerical computation.

The derived approximate equilibrium length scales of the system were used to generate element-based orthogonal collocation grids for both transient (5 elements) and steady-state (4 elements) PBE. Grids of different sizes were evaluated by comparing them to the available analytical solution as well as checking the numerical value for the volume fraction deviation.

The results suggest that number of collocation points between 10 and 20 can be selected by a trade-off between the desired accuracy and computation time. The iterative scheme for steady-state PBE does not provide sufficient accuracy. Alternatively, a transient solution from the initial distribution as the estimated equilibrium distribution is recommended. This approach has decreased the required computational time by around 40–70% for the studied cases.

The above evidence suggests that the technique has high potential to address the well-known computational efficiency and robustness challenges associated with the numerical solution of PBEs. In our future publications, we will address these issues for more complex systems.

Declaration of Competing Interest

The authors declare that they have no known competing financial interests or personal relationships that could have appeared to influence the work reported in this paper.

Acknowledgments

This work was carried out as a part of SUBPRO, a Research-Based Innovation Center within Subsea Production and Processing. The authors gratefully acknowledge the financial support from SUBPRO, which is financed by the Research Council of Norway, major industry partners, and NTNU.

Appendix A. Supporting information

Supplementary data associated with this article can be found in the online version at doi:10.1016/j.cherd.2022.10.044.

References

Attarakih, M.M., Bart, H.J., Faqir, N.M., 2002. An approximate optimal moving grid technique for the solution of discretized population balances in batch. Comput. Aided Chem. Eng. 823–828. https://doi.org/10.1016/S1570-7946(02)80165-1

Attarakih, M.M., Bart, H.J., Faqir, N.M., 2004. Numerical solution of the spatially distributed population balance equation describing the hydrodynamics of interacting liquid-liquid dispersions. Chem. Eng. Sci. 59, 2567–2592. https://doi.org/10.1016/j.ces.2004.03.005

Benjamin, B.J., Madras, G., 2003. Analytical solution for a population balance equation with aggregation and fragmentation. Chem. Eng. Sci. 58, 3049–3051. https://doi.org/10.1016/S0009-2509(03)00159-3

Briesen, H., 2009. Adaptive moving pivot technique for growth dominated population balance equations. Comput. Aided Chem. Eng. 26, 895–900. https://doi.org/10.1016/S1570-7946(09)70149-X

Chesters, A.A., 1991. The modelling of coalescence processes in fluid-liquid dispersions: a review of current understanding. Chem. Eng. Res. Des. 69, 259–270.

Costa, L.I., Storti, G., Lazzari, S., 2018. Solution of population balance equations by logarithmic shape preserving interpolation on finite elements. Comput. Chem. Eng. 119, 13–24. https://doi.org/10.1016/j.compchemeng.2018.08.008

Coulaloglou, C.A., Tavlarides, L.L., 1977. Description of interaction processes in agitated liquid-liquid dispersions. Chem. Eng. Sci. 32, 1289–1297. https://doi.org/10.1016/0009-2509(77)85023-9

Dorao, C.A., Jakobsen, H.A., 2006. A least squares method for the solution of population balance problems. Comput. Chem. Eng. 30, 535–547. https://doi.org/10.1016/j.compchemeng.2005.10.012

Duarte, B.P.M., Baptista, C.M.S.G., 2007. Using moving finite elements method to solve population balance equations comprising breakage terms. Comput. Aided Chem. Eng. 24, 255–260. https://doi.org/10.1016/S1570-7946(07)80066-6

Eskin, D., Taylor, S., Ma, S.M., Abdallah, W., 2017. Modeling droplet dispersion in a vertical turbulent tubing flow. Chem. Eng. Sci. 173, 12–20. https://doi.org/10.1016/j.ces.2017.07.023

Falola, A., Borissova, A., Wang, X.Z., 2013. Extended method of moment for general population balance models including size dependent growth rate, aggregation and breakage kernels. Comput. Chem. Eng. 56, 1–11. https://doi.org/10.1016/j.compchemeng.2013.04.017

Filbet, F., Laurençot, P., 2004. Numerical simulation of the Smoluchowski coagulation equation. SIAM J. Sci. Comput. 25, 2004–2028. https://doi.org/10.1137/S1064827503429132

Fritsch, F.N., Carlson, R.E., 1980. Monotone Piecewise cubic interpolation. SIAM J. Numer. Anal. 17, 238–246. https://doi.org/10.1137/0717021

Gelbard, F., Seinfeld, J.H., 1978. Numerical solution of the dynamic equation for particulate systems. J. Comput. Phys. 28, 357–375. https://doi.org/10.1016/0021-9991(78)90058-X

Hsia, M.A., Tavlarides, L.L., 1983. Simulation analysis of drop breakage, coalescence and micromixing in liquid-liquid stirred tanks. Chem. Eng. J. 26, 189–199. https://doi.org/10.1016/0300-9467(83)80014-8

Kumar, S., Ramkrishna, D., 1996a. On the solution of population balance equations by discretization - I. A fixed pivot technique. Chem. Eng. Sci. 51, 1311–1332. https://doi.org/10.1016/0009-2509(96)88489-2

Kumar, S., Ramkrishna, D., 1996b. On the solution of population balance equations by discretization - II. A moving pivot technique. Chem. Eng. Sci. 51, 1333–1342. https://doi.org/10.1016/0009-2509(95)00355-X

Lee, G., Yoon, E.S., Young-Il Lim, Jean Marc Le. Lann, Xuân-Mi Meyer, A., Joulia, X., 2001. Adaptive mesh method for the simulation of crystallization processes including agglomeration and breakage: the potassium sulfate system. Ind. Eng. Chem. Res. 40, 6228–6235. https://doi.org/10.1021/IE010443R

Mahoney, A.W., Ramkrishna, D., 2002. Efficient solution of population balance equations with discontinuities by finite elements. Chem. Eng. Sci. 57, 1107–1119. https://doi.org/10.1016/S0009-2509(01)00427-4

Mantzaris, N.V., Daoutidis, P., Srienc, F., 2001a. Numerical solution of multi-variable cell population balance models. II. Spectral methods. Comput. Chem. Eng. 25, 1441–1462. https://doi.org/10.1016/S0098-1354(01)00710-4

Mantzaris, N.V., Daoutidis, P., Srienc, F., 2001b. Numerical solution of multi-variable cell population balance models. III. Finite element methods. Comput. Chem. Eng. 25, 1463–1481. https://doi.org/10.1016/S0098-1354(01)00711-6

Nicmanis, M., Hounslow, M.J., 1996. A finite element analysis of the steady state population balance equation for particulate systems: aggregation and growth. Comput. Chem. Eng. 20, S261–S266. https://doi.org/10.1016/0098-1354(96)00054-3

Nicmanis, M., Hounslow, M.J., 1998. Finite-element methods for steady-state population balance equations. AIChE J. 44, 2258–2272. https://doi.org/10.1002/aic.690441015

Prince, M.J., Blanch, H.W., 1990. Bubble coalescence and break-up in air-sparged bubble columns. Aiche J. 36, 1485–1499. https://doi.org/10.1002/aic.690361004

Qamar, S.M., 2014. Application of the method of characteristics to population balance models considering growth and nucleation phenomena. Appl. Math. 5, 1853–1862. https://doi.org/10.4236/am.2014.513178

Ramkrishna, D., 2000. Population Balances: Theory and Applications to Particulate Systems in Engineering. Academic Presshttps://doi.org/10.1016/B978-0-12-576970-9.X5000-0

Rigopoulos, S., Jones, A.G., 2003. Finite-element scheme for solution of the dynamic population balance equation. AIChE J. 49, 1127–1139. https://doi.org/10.1002/aic.690490507

Sewerin, F., Rigopoulos, S., 2017. An explicit adaptive grid approach for the numerical solution of the population balance equation. Chem. Eng. Sci. 168, 250–270. https://doi.org/10.1016/j.ces.2017.01.054

Solsvik, J., Jakobsen, H.A., 2012. Effects of Jacobi polynomials on the numerical solution of the pellet equation using the orthogonal collocation, Galerkin, tau and least squares methods. Comput. Chem. Eng. 39, 1–21. https://doi.org/10.1016/j.compchemeng.2011.11.015

Solsvik, J., Jakobsen, H.A., 2013. Evaluation of weighted residual methods for the solution of a population balance model describing bubbly flows: the least-squares, Galerkin, Tau, and

orthogonal collocation methods. Ind. Eng. Chem. Res. 52 (45), 15988–16013. https://doi.org/10.1021/ie402033b

Vankova, N., Tcholakova, S., Denkov, N.D., Vulchev, V.D., Danner, T., 2007. Emulsification in turbulent flow. 2. Breakage rate constants. J. Colloid Interface Sci. 313, 612–629. https://doi.org/10.1016/J.JCIS.2007.04.064

Villadsen, J., Michelsen, M.L., 1978. Solution of Differential Equation Models by Polynomial Approximation. Prentice-Hall, Englewood Cliffs, New York.

Zhu, Z., Dorao, C.A., Jakobsen, H.A., 2008. A least-squares method with direct minimization for the solution of the breakage-coalescence population balance equation. Math. Comput. Simul. 79, 716–727. https://doi.org/10.1016/j.matcom.2008.05.001

Zhu, Z., Dorao, C.A., Lucas, D., Jakobsen, H.A., 2009. On the coupled solution of a combined population balance model using the least-squares spectral element method. Ind. Eng. Chem. Res. 48, 7994–8006. https://doi.org/10.1021/ie900088q